VI International Conference on Computational Methods for Coupled Problems in Science and Engineering
COUPLED PROBLEMS 2015
B. Schrefler, E. Oñate and M. Papadrakakis(Eds)

MIGRATION OF A RIGID DISC IN COUETTE FLOW SUBJECT TO AN EXTERNAL ELECTRIC FIELD SIMULATED USING ISPH

NIMA TOFIGHI[†], MURAT OZBULUT[†], AMIN RAHMAT[†], JAMES J. FENG[‡] AND MEHMET YILDIZ[†]

[†]Faculty of Engineering and Natural Sciences (FENS), Sabanci University,
Orhanli, Tuzla, 34956 Istanbul, Turkey
e-mails: nima@sabanciuniv.edu
ozbulut@sabanciuniv.edu
arahmat@sabanciuniv.edu
meyildiz@sabanciuniv.edu

[‡]Department of Mathematics and Department of Chemical and Biological Engineering,
University of British Columbia, Vancouver, BC V6T 1Z2, Canada
e-mail: james.feng@ubc.ca

Key words: Smoothed Particle Hydrodynamics, Fluid Solid Interaction, Electrohydrodynamics, Disc Migration

Abstract. Incompressible smoothed particle hydrodynamics method has been used to simulate the migration of a two-dimensional rigid disc in Couette flow in presence of an external electric field. The electric field is perpendicular to the moving walls. The results show that the trajectory of the disc is affected by the electrical properties of fluid and solid.

1 INTRODUCTION

The interaction of a solid body with a fluid environment is one of the most common flow features in nature and industry. When exposed to an external electric field, the motion of the solid may undergo significant changes. Migration of rigid discs in Couette flow has been the subject of many studies [1–3]. On the other hand, the rotation of spherical bodies in electric field known as Quincke rotation [4], has attracted much attention [5, 6]. It is known that a particle laden fluid may exhibit changing viscosity when exposed to an external electric field [7, 8]. This behavior is attributed to changing motion of particles due to the electric field. However, a fully resolved simulation of a disc migrating in electric field has not been conducted.

In this study, a two-dimensional Incompressible Smoothed Particle Hydrodynamics (ISPH) scheme is used to simulate the motion of a rigid disc in Couette flow subject to an external electric field [9]. Solid and fluid phases are modeled as leaky dielectric materials [10] while the electric field is taken to be perpendicular to the moving walls and in-plane with the flow. Numerical simulation of a single disc placed off-center in Couette flow is carried out and the results are validated against literature data in the absence of an electric field. Then the same case at different electric permittivity and conductivity ratios is simulated and compared to the case with no electric field. The results show that when the conditions for Quincke rotation are satisfied, the disc's migration toward the channel's center is hindered, in agreement with experiments [11].

2 GOVERNING EQUATIONS

Equations governing an incompressible flow subject to an external electric field may be written in dimensionless form as

$$\boldsymbol{\nabla} \cdot \mathbf{u} = 0, \tag{1}$$

$$\frac{\mathrm{D}\mathbf{u}}{\mathrm{D}t} = -\frac{1}{\rho}\boldsymbol{\nabla} p + \frac{1}{\mathrm{Re}}\boldsymbol{\nabla} \cdot \boldsymbol{\tau} + \frac{1}{\mathrm{Ei}}\mathbf{f}_{(e)}, \tag{2}$$

where $\mathbf{u}$ is the velocity vector, p is pressure, ρ is density, t is time and $\mathrm{D}/\mathrm{D}t = \partial/\partial t + \mathbf{u}\cdot\boldsymbol{\nabla}$ represents the material time derivative. Here, $\boldsymbol{\tau}$ is the viscous stress tensor,

$$\boldsymbol{\tau} = \mu\left[\boldsymbol{\nabla}\mathbf{u} + (\boldsymbol{\nabla}\mathbf{u})^{\dagger}\right], \tag{3}$$

where μ denotes viscosity and superscript $\square^{\dagger}$ represents the transpose operation. $\mathbf{f}_{(e)}$ is the electric force vector defined as [10]

$$\mathbf{f}_{(e)} = -\frac{1}{2}\mathbf{E}\cdot\mathbf{E}\boldsymbol{\nabla}\varepsilon + q^{v}\mathbf{E}. \tag{4}$$

Here ε denotes electric permittivity, q^{v} is is the volume charge density near the interface while $\mathbf{E}$ is the electric field vector. Assuming small dynamic currents and neglecting magnetic induction effects, the electric field is irrotational [12] and may be represented by gradient of an electric potential ϕ, $\mathbf{E} = -\boldsymbol{\nabla}\phi$. Further assumption of fast electric relaxation time compared to viscous relaxation time leads to the following relations for electric potential and charge density

$$\boldsymbol{\nabla}\cdot(\sigma\boldsymbol{\nabla}\phi) = 0, \tag{5}$$

$$q^{v} = \boldsymbol{\nabla}\cdot(\varepsilon\boldsymbol{\nabla}\phi), \tag{6}$$

where σ is the electrical conductivity.

Dimensionless values are formed using the following scales

$$\begin{aligned} &\mathbf{x} = \mathbf{x}^*/a, \quad \rho = \rho^*/\rho_f, \quad \mathbf{u} = \mathbf{u}^*/Ga, \quad t = t^*G, \\ &\mathbf{E} = \mathbf{E}^*/E_\infty, \quad \phi = \phi^*/E_\infty H, \quad p = p^*/\rho_f \left(Ga\right)^2, \\ &\mathcal{R} = \rho_s/\rho_f, \quad \mathcal{M} = \mu_s/\mu_f, \quad \mathcal{P} = \varepsilon_s/\varepsilon_f, \quad \mathcal{C} = \sigma_s/\sigma_f, \quad \mathcal{D} = a/H \end{aligned} \tag{7}$$

leading to Reynolds and inverse Electroinertial numbers defined as

$$\mathrm{Re} = \frac{\rho_f G a^2}{\mu_f}, \quad \mathrm{Ei} = \frac{\rho_f \left(Ga\right)^2}{\varepsilon_f E_\infty^2}. \tag{8}$$

Here E_∞ is the undisturbed electric field intensity, H is the distance between electrodes, G is the shear rate and a denotes disc radius (figure 1-a). An asterisk marks dimensional variables whereas subscripts $\square_s$ and $\square_f$ denote fluid and solid phases, respectively.

To distinguish between different phases, a color function $\hat{c}$ is defined such that it assumes a value of zero for one phase and unity for the other. The color function is then smoothed out across the phase boundaries as

$$c_\mathrm{i} = \sum_{\mathrm{j}=1}^{J_n} \frac{\hat{c}_\mathrm{j} W_\mathrm{ij}}{\psi_\mathrm{i}}, \tag{9}$$

to ensure smooth transition between the properties of each phase when used for their interpolation. Here, $\psi_\mathrm{i} = \sum_{\mathrm{j}=1}^{J_n} W_\mathrm{ij}$, is the number density of SPH particle i, calculated as the sum of interpolation kernel of neighboring particles i and j over all neighbors of particle i, J_n. Interpolation kernel, $W(r_\mathrm{ij}, h)$, is a function of the magnitude of distance vector, $\mathbf{r}_\mathrm{ij} = \mathbf{r}_\mathrm{i} - \mathbf{r}_\mathrm{j}$, between particle of interest i and its neighboring particles j and h, the smoothing length [13, 14]. Interpolation of phase properties is carried out using Weighted Harmonic Mean (WHM),

$$\frac{1}{\chi_\mathrm{i}} = \frac{c_\mathrm{i}}{\chi_s} + \frac{1 - c_\mathrm{i}}{\chi_f}, \tag{10}$$

where χ may denote density, viscosity, permittivity or conductivity [15].

All phases are treated as liquids initially while additional rigidity constraints are imposed in solid region [9]. To this end we use the current velocity of the solid particles to compute a center-of-mass velocity and an angular velocity for the solid object:

$$\mathbf{u}_s^t = \frac{1}{J_s} \sum_{\mathrm{j}=1}^{J_s} \mathbf{u}_\mathrm{j}, \quad \mathbf{u}_s^r = \frac{1}{I_s} \sum_{\mathrm{j}=1}^{J_s} \mathbf{u}_\mathrm{j} \times \mathbf{r}_{\mathrm{j}s}, \tag{11}$$

and then assign an individual velocity to each solid particle according to rigid body motion:

$$\mathbf{u}_\mathrm{i} = \mathbf{u}_s^t + \mathbf{u}_s^r \times \mathbf{r}_{\mathrm{i}s}. \tag{12}$$

Here, $\mathbf{r}_{is} = \mathbf{r}_i - \mathbf{r}_s$ where $\mathbf{r}_s$ denotes the solid object's center of mass, J_s is the number of particles present in the solid phase and I_s is the solid object's moment of inertia about its center of mass.

A predictor-correcter scheme is employed to advance the governing equations in time using a first-order Euler approach with variable timestep according to Courant-Friedrichs-Lewy condition, $\Delta t = C_{CFL} h/u_{max}$, where u_{max} is the largest particle velocity magnitude and C_{CFL} is taken to be equal to 0.25. In the predictor step, equations (5) and (6) are solved to obtain $\mathbf{f}_{(e)}^{(n)}$ through equation (4). Then position, velocity and number density are advanced to their intermediate forms using the following relations,

$$\mathbf{r}_i^+ = \mathbf{r}_i^{(n)} + \mathbf{u}_i^{(n)} \Delta t + \boldsymbol{\delta}\mathbf{r}_i^{(n)}, \tag{13}$$

$$\mathbf{u}_i^+ = \mathbf{u}_i^{(n)} + \left(\frac{1}{\mathrm{Re}} \boldsymbol{\nabla} \cdot \boldsymbol{\tau}_i^{(n)} + \frac{1}{\mathrm{Ei}} \mathbf{f}_{(e),i}^{(n)} \right) \Delta t, \tag{14}$$

$$\psi_i^+ = \psi_i^{(n)} - \Delta t \psi_i^{(n)} \left(\boldsymbol{\nabla} \cdot \mathbf{u}_i^+ \right), \tag{15}$$

where starred variables represent intermediate values and superscript (n) denotes values at the n^{th} time step. The artificial particle displacement vector in equation (13), $\boldsymbol{\delta}\mathbf{r}_i$, is defined as in [16] and a constant value of 0.06 is used.

Using intermediate values, pressure at the next time step is found by solving the Poisson equation. This is then followed by corrections in position and velocity of the particles, completing the temporal transition:

$$\boldsymbol{\nabla} \cdot \left(\frac{1}{\rho_i^+} \boldsymbol{\nabla} p_i^{(n+1)} \right) = \frac{\boldsymbol{\nabla} \cdot \mathbf{u}_i^+}{\Delta t}, \tag{16}$$

$$\mathbf{u}_i^{(n+1)} = \mathbf{u}_i^+ - \frac{1}{\rho_i} \boldsymbol{\nabla} p_i^{(n+1)} \Delta t, \tag{17}$$

$$\mathbf{r}_i^{(n+1)} = \mathbf{r}_i^{(n)} + \frac{1}{2} \left(\mathbf{u}_i^{(n)} + \mathbf{u}_i^{(n+1)} \right) \Delta t + \boldsymbol{\delta}\mathbf{r}_i^{(n)}. \tag{18}$$

In these equations, the rigidity constraints (equations (11) and (12)) are implemented after each velocity update.

Boundary conditions are enforced through the MBT method described in [17] while the first derivative and the Laplace operator are approximated through the following expressions

$$\frac{\partial f_i^m}{\partial x_i^k} a_i^{kl} = \sum_j \frac{1}{\psi_j} \left(f_j^m - f_i^m \right) \frac{\partial W_{ij}}{\partial x_i^l}, \tag{19}$$

$$\frac{\partial^2 f_i^m}{\partial x_i^k \partial x_i^k} a_i^{ml} = 8 \sum_j \frac{1}{\psi_j} \left(f_i^m - f_j^m \right) \frac{r_{ij}^m}{r_{ij}^2} \frac{\partial W_{ij}}{\partial x_i^l}. \tag{20}$$

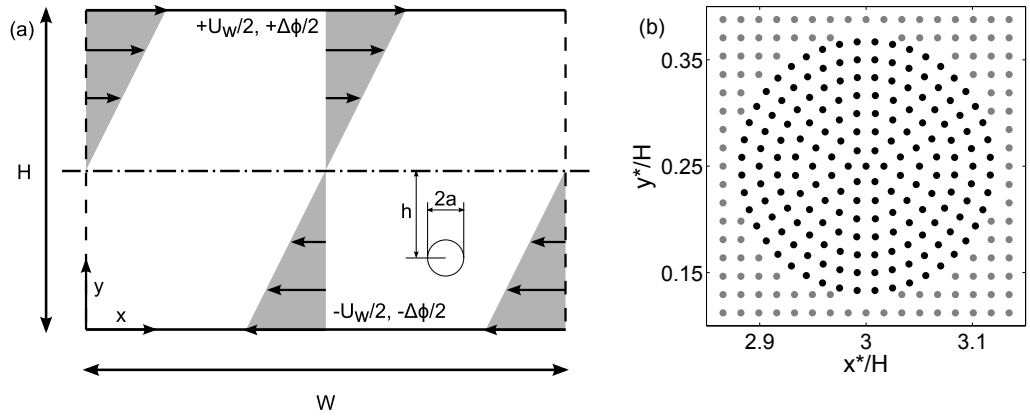

Figure 1: (a) Schematic of the test case. (b) Closeup view of initial particle distribution at the vicinity of the solid disc. Black points denote solid particles whereas gray points are fluid particles.

Here, $a_{\mathrm{i}}^{kl} = \sum_{\mathrm{j}} \frac{r_{\mathrm{ij}}^k}{\psi_{\mathrm{j}}} \frac{\partial W_{\mathrm{ij}}}{\partial x_{\mathrm{i}}^l}$ is a corrective second rank tensor that eliminates particle inconsistencies [16]. The left hand side of equation (16) is discretized as

$$\frac{\partial^2 f_{\mathrm{i}}^m}{\partial x_{\mathrm{i}}^k \partial x_{\mathrm{i}}^k} \left(2 + a_{\mathrm{i}}^{kk}\right) = 8 \sum_{\mathrm{j}} \frac{1}{\psi_{\mathrm{j}}} \left(f_{\mathrm{i}}^m - f_{\mathrm{j}}^m\right) \frac{r_{\mathrm{ij}}^k}{r_{\mathrm{ij}}^2} \frac{\partial W_{\mathrm{ij}}}{\partial x_{\mathrm{i}}^k}. \tag{21}$$

3 RESULTS

In this study, migration of a neutrally buoyant rigid disc in plane Couette flow is simulated. When released from a distance h from the middle of the channel, it is expected that the disc will migrate toward the centerline while moving with the flow for $\mathrm{Re} \leq 2$ [1, 18]. A schematic of this case is provided in figure 1-a. Computational domain consists of an 8×32 rectangle discretized by 13806 particles initially arranged in a Cartesian grid for fluid and concentric circles for the solid [9]. A close-up view of the particle arrangement at the vicinity of the solid disc is provided in figure 1-b. The confinement ratio is $\mathcal{D} = 0.125$ while the disc is placed at $h/H = 0.25$ below the centerline. Top and bottom walls abide by no-slip condition and are moving in opposite directions at a velocity of $U_w/2$ where $U_w = GH$. Periodic boundary condition is imposed in streamwise direction. Using a viscosity ratio of 100 [9] the results are compared to literature data in the absence of electric field at $\mathrm{Re} = 0.625$. Figure 2 shows the vertical position of the disc versus time. As it is seen, the results of the current simulation are in good agreement with the results found in [1–3].

When exposed to an external electric field, the motion of the disc may be altered depending on the properties of the fluid and solid. To investigate the effects, Ei is set to Re/4 to provide a large enough electric force while Re is kept equal to 0.625. A constant electric potential difference of $\Delta\phi = E_\infty H$ is imposed between the moving walls, resulting in an electric field perpendicular to the flow, while periodic boundary condition is imposed

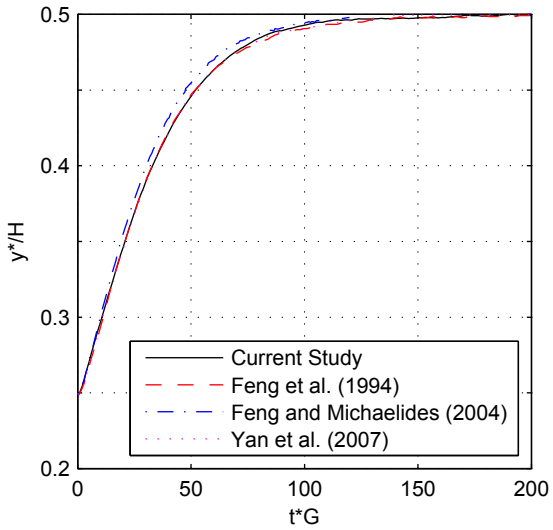

Figure 2: Comparison of the vertical position of the disc's center of mass versus time in the absence of electric field.

in streamwise direction. Permittivity and conductivity ratios are individually varied as 0.2, 0.5, 2 and 5 (table 1). When $\mathcal{P} = \mathcal{C}$, the leaky dielectric model is reduced to the perfect dielectric model. As such, equal permittivity and conductivity ratios are avoided here. Figure 3 plots the trajectory and velocity of the disc for the case without electric field and for $(\mathcal{P}, \mathcal{C})$ pairs of $(0.2, 5)$ and $(5, 0.2)$. The disc in case $(0.2, 5)$ is accelerated toward the centerline while in case $(5, 0.2)$ it is moved toward the wall. Case $(5, 0.2)$ is solved until the disc touches the bottom wall. Defining $\tau = \varepsilon/\sigma$ as the electric time scale, the necessary condition for Quincke rotation is $\tau_f < \tau_s$ [6]. The configuration of electric forces in case $(5, 0.2)$ is such that the condition for Quincke rotation is satisfied. This results in an angular moment that assists the rotation of the disc in the flow. On the other hand, case $(0.2, 5)$ has reduced angular velocity compared to the case with no electric field. Normal velocity becomes zero when disc hits bottom wall or reaches the channel centerline.

Table 1 provides the time until the disc comes to one radius distance of the bottom wall or the channel center. Bold numbers show that the disc approaches the bottom wall. The disc reaches the channel center at $t^*G = 25.94$ when no electric field is applied. When $\tau_f > \tau_s$ (lower triangle), the disc travels faster toward the channel center while when $\tau_f < \tau_s$ (upper triangle) the disc travels slower toward the channel center or moves toward the channel wall. Such observations are reported in experiments as well [11]. As it is seen, increasing the permittivity ratio at a constant conductivity ratio results in a gradual increase in the time needed for the disc to reach the channel center. At large enough permittivity ratios the trajectory is reversed and the disc migrates toward the channel wall. At this point, further increase of the permittivity ratio results in a

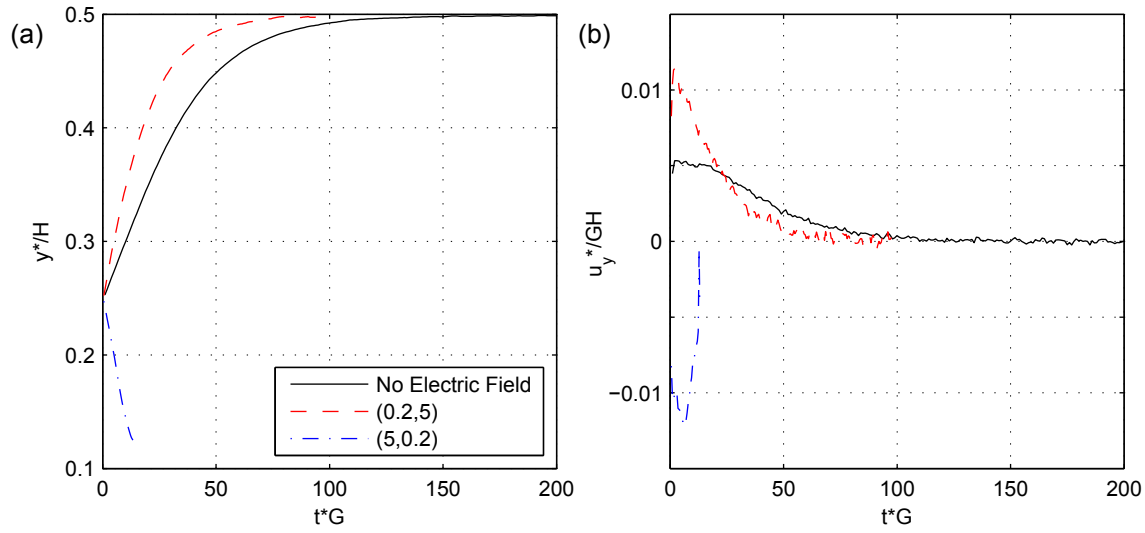

Figure 3: Comparison of the vertical position (a) and vertical velocity (b) of the disc's center of mass versus time.

Table 1: Time until the disc reaches one radius distance of channel center (regular) or bottom wall (bold). The disc reaches channel center at $t^*G = 25.94$ when no electric field is applied.

$\mathcal{P}$		0.2	0.5	2	5
$\mathcal{C}$	0.2	-	80.05	**19.18**	**13.34**
	0.5	17.79	-	**44.89**	**29.37**
	2	13.49	17.18	-	33.59
	5	13.81	16.89	24.07	-

faster migration toward the channel wall. The inverse of this trend is observed when the permittivity ratio is kept constant and the conductivity ratio is increased.

4 CONCLUSION

In this paper, we use ISPH to simulate the migration of a rigid disc in Couette flow under external electric field. The results of the case without electric field are compared to literature data and good agreement is observed. Further simulations are carried out at different permittivity and conductivity ratios and the results are compared to the case with no electric field. When the electric field augments the rotation of the disc, its motion toward the center of the channel is hindered. At large enough ratios, this results in complete reversal of the motion as the disc approaches the channel wall. Conversely the disc moves faster toward the center when its angular motion is hindered.

5 ACKNOWLEDGMENTS

The authors gratefully acknowledge financial support provided by the Scientific and Technological Research Council of Turkey (TUBITAK) for project number 112M721 and by the Natural Sciences and Engineering Research Council (NSERC) of Canada.

REFERENCES

[1] Feng, J., Hu, H.H. and Joseph, D.D. Direct simulation of initial-value problems for the motion of solid bodies in a Newtonian fluid .2. Couette and Poiseuille flows. *J. Fluid Mech.* (1994) **277**:271-301.

[2] Feng, Z.G. and Michaelides, E.E. The immersed boundary-lattice Boltzmann method for solving fluid-particles interaction problems. *J. Comput. Phys.* (2004) **195**:602-628.

[3] Yan, Y., Morris, J.F. and Koplik, J. Hydrodynamic interaction of two particles in confined linear shear flow at finite Reynolds number. *Phys. Fluids* (2007) **19**:113305.

[4] Quincke, G. Ueber rotationen im constanten electrischen felde. *Annalen der Physik* (1896) **295**:417-486.

[5] Peters, F., Lobry, L., Khayari, A. and Lemaire, E. Size effect in Quincke rotation: A numerical study. *J. Chem. Phys.* (2009) **130**:194905.

[6] Das, D. and Saintillan, D. Electrohydrodynamic interaction of spherical particles under Quincke rotation. *Phys. Rev. E* (2013) **87**:043014.

[7] Pannacci, N., Lemaire, E. and Lobry, L. Rheology and structure of a suspension of particles subjected to Quincke rotation. *Rheol. Acta* (2007) **46**:899-904.

[8] Huang, H.F., Zahn, M. and Lemaire, E. Continuum modeling of micro-particle electrorotation in Couette and Poiseuille flows-The zero spin viscosity limit. *J. Electrost.* (2010) **68**:345-359.

[9] Tofighi, N., Ozbulut, M., Rahmet, A., Yildiz, M. and Feng, J.J. Descent of a solid disk in quiescent fluid simulated using incompressible smoothed hydrodynamics. *Proceedings of WCCM XI* (2014) **5**:5310-5318.

[10] Saville, D. Electrohydrodynamics: The Taylor-Melcher leaky dielectric model. *Annu. Rev. Fluid Mech.* (1997) **29**:27-64.

[11] Boissy, C., Atten, P. and Foulc, J. On a negative rheological effect. *J. Electrost.* (1995) **35**:13-20.

[12] Hua, J., Lim, L. and Wang, C. Numerical simulation of deformation/motion of a drop suspended in viscous liquids under influence of steady electric fields. *Phys. Fluids* (2008) **20**:113302.

[13] Monaghan, J.J. and Lattanzio, J.C. A refined particle method for astrophysical problems. *Astron. Astrophys.* (1985) **149**:135–143.

[14] Monaghan, J.J. and Kocharyan, A. SPH simulation of multiphase flow. *Comput. Phys. Commun.* (1995) **87**:225–235.

[15] Tomar, G., Gerlach, D., Biswas, G., Alleborn, N., Sharma, A., Durst, F., Welch, S.W.J. and Delgado, A. Two-phase electrohydrodynamic simulations using a volume-of-fluid approach. *J. Comput. Phys.* (2007) **227**:1267-1285.

[16] Zainali, A., Tofighi, N., Shadloo, M.S. and Yildiz, M. Numerical investigation of Newtonian and non-Newtonian multiphase flows using ISPH method. *Comput. Meth. Appl. Mech. Eng.* (2013) **254**:99–113.

[17] Yildiz, M., Rook, R.A. and Suleman, A. SPH with the multiple boundary tangent method. *Int. J. Numer. Methods Eng.* (2009) **77**:1416–1438.

[18] Pan, T.W., Huang, S.L., Chen, S.D., Chu, C.C. and Chang, C.C. A numerical study of the motion of a neutrally buoyant cylinder in two dimensional shear flow. *Comput. Fluids* (2013) **87**:57-66.